Application of an integrated geotechnical and topographic monitoring system in the Lorano marble quarry (Apuan Alps, Italy)

Riccardo Salvini[a,*], Claudio Vanneschi[a], Silvia Riccucci[a], Mirko Francioni[b], Domenico Gullì[c]

[a]*Department of Environment, Earth and Physical Sciences and Centre of Geotechnologies, University of Siena, Via Vetri Vecchi 34, 52027 San Giovanni Valdarno, Italy, e-mail: riccardo.salvini@unisi.it, claudio.vanneschi@unisi.it, riccucci8@unisi.it*

[b]*Department of Earth Sciences, Simon Fraser University, 8888 University Drive, Burnaby BC, V5A 1S6, Canada, e-mail: mfrancio@sfu.ca*

[c]*USL1 Massa and Carrara - Mining Engineering Operative Unit - Department of Prevention, Via Don Minzoni 3, 54033 Carrara, Italy, e-mail: d.gulli@usl1.toscana.it*

*Corresponding author. Tel.: +39 055 9119441. E-mail address: riccardo.salvini@unisi.it (R. Salvini)

Abstract

Accurate slope stability analysis is essential for human activity in high-risk geological contexts. This may, however, not be enough in the case of quarrying where the dynamic and evolving environment also requires effective monitoring. A well-designed monitoring system requires the acquisition of a huge dataset over time, improving knowledge of the study area and helping to refine prediction from stability analysis.

This paper reports the implementation of an integrated monitoring system in a marble quarry in the Apuan Alps (Italy) and some of the results obtained. The equipment consists of a traditional geotechnical monitoring system (extensometers, crackmeters and clinometers) and two modern topographic monitoring systems (a terrestrial interferometer and a robotic total station). This work aims to provide in-depth knowledge of the large scale rock mass behavior as a result of marble exploitation, thereby allowing continuous excavation. The results highlight the importance of integrating different monitoring systems.

Keywords: Marble quarry; Slope stability; Rock buttress; Monitoring system; Robotic total station; Displacement analysis.

1. Introduction

The use of monitoring systems to assess and predict geological hazards, especially rockfall, and correctly plan future excavation activities is becoming an established practice to protect quarry workers. However, the deployment of an adequate monitoring system is often impossible due to a lack of scientific experience and funding. In addition, instrumental monitoring may not be feasible unless only a small area is examined for specific purposes (Wieczorek and Snyder, 2009).

The impact of human factors on slope stability has been indicated for the Vajont rockslide, Italy (Semenza, 1965), and other events that have recently occurred all over the world (e.g., Griffiths et al., 2004; Sarwar, 2008; Robbins et al., 2013; Pankow et al., 2014). A monitoring system for early-warning of rock failure needs to consider this aspect. There are different types of monitoring systems with varied accuracy, invasiveness, field of view, distance range and cost. There is no universal monitoring system because of different geological, morphological, physical or human factors among sites (Wieczorek and Snyder, 2009).

Slope stability studies may be complex and even hazardous to undertake in certain environments such as quarries with tall walls. The problems can be overcome by using remote sensing techniques like digital terrestrial photogrammetry (DTP) and terrestrial laser scanning (TLS) (Sturzenegger and Stead, 2009; Firpo et al., 2011; Fekete and Diederichs, 2013; Salvini et al., 2013, 2014a, b), this provides a basis for selecting and installing appropriate monitoring systems. Geotechnical monitoring systems such as extensometers, crackmeters and clinometers have also been successfully integrated with topographic instruments such as ground-based InSAR (interferometric synthetic aperture radar) (e.g., Schulz et al., 2012; Kristensen et al., 2013), TLS (e.g., Aryal, 2013; Teza et al., 2014), GPS (global positioning system) (e.g., Liu et al., 2004; Gigli et al., 2011; Kenner et al., 2014), and total station (e.g., Kuhlmann and Glaser, 2002; Tsai et al., 2011; Giordan et al., 2013).

The present study deals with a quarry in the Apuan Alps marble district (Fig. 1), which is characterized by several artificial high walls often located at the bottom of natural slopes with complex morphologies. In this context, it is important to characterise and reduce geological risk for the safety of the workforce. This study conducted engineering geological surveys in accessible areas and used remote sensing techniques (DTP and TLS) in inaccessible areas (Salvini et al. 2014a, b). An integrated monitoring system with three components was installed, comprising: a terrestrial interferometer operated by “La Sapienza” University of Rome from July to December 2012, a geotechnical system operated by USL1 of Massa and Carrara and “*Cooperativa Cavatori Lorano*” since July 2012, and a robotic total station (RTS) run by the University of Siena since November 2012 (Salvini et al. 2014c). This paper describes the monitoring systems and analyses the findings, focusing on data collected by the RTS.

2. Geographical and geological setting

The Lorano quarry is located in the Province of Massa and Carrara, northwestern Tuscany (Italy). In 1997, a rockfall occurred in the quarry resulting in an interruption to excavation activities for a few weeks. Remediation works were subsequently carried out, with the aim of ensuring safe conditions in the quarry, and a marble buttress accessible from three sides was emplaced (Fig. 1). Due to the ongoing quarrying activity at present the buttress is about 150 m high, 30 m wide and 40 m thick.

The quarry is located in a fold-and-thrust belt of the Northern Apennines, derived from the Tertiary collision (66 Ma) between the Sardinia-Corsica block and the Adria plate (Boccaletti et al., 1971; Scandone, 1979; Dercourt et al., 1986). With the closure of the Ligurian sector of the Ligurian-Piemontese ocean, the Ligurian and sub-Ligurian accretionary wedge was thrust above the external

Tuscan and Umbria-Marche domains (Elter, 1975; Marroni et al., 2010). The Apuan Alps metamorphic complex (Fig. 2), first described by Zaccagna (1932), represents one of the deepest structural levels in the inner portion of the orogenic belt and consists of two main tectono-metamorphic units, the Massa and Apuan. The Massa Unit is well exposed in the westernmost part of the Apuan Alps, represented by a Paleozoic basement and an Upper Permian-Upper Triassic sedimentary succession. The quarry is located in the Apuan Unit, made up of the Paleozoic basement unconformably overlain by the Upper Triassic–Oligocene metasedimentary sequence. The basement is exposed in large outcrops, composed of the Upper Cambrian–Lower Ordovician phyllites and quarzites with intercalated mafic volcanic rocks; Middle Ordovician metavolcanics and metavolcanoclastics; Upper Ordovician quartzic metasandstones and phyllites; Silurian black phyllites and Orthoceras-bearing metadolostones; and Lower Devonian calcschists (Gattiglio et al., 1989; Conti et al., 1993). The basement rocks recorded pre-Alpine deformation and greenschist-facies metamorphism. The Mesozoic cover-rocks include thin Triassic continental to shallow marine Verrucano-like deposits followed by Upper Triassic–Liassic carbonate platform metasediments comprised of dolomites and marbles; and Upper Liassic–Lower Cretaceous cherty metalimestones, radiolarian cherts and calcschists (Conti et al., 2004).

The two major tectonic events of the Apuan Alps, D1 and D2, were identified in the metamorphic complex (Carmignani et al., 1980; Carmignani and Kligfield, 1990). The D1 phase is related to ductile compression due to the continental collision between the Sardinia-Corsica block and the Adria plate. Deformation structures generated by the compression are easily identified in the northern Apuan Alps, including kilometric thrusts, isoclinal folds, regional greenschist foliations (S_1) that often completely transpose the original stratification, and SW–NE oriented stretching lineations (L_1) interpreted as the main transport direction of the inner Northern Apennines (Carmignani et al., 1978; Molli, 2008). The S_1 schistosity is parallel to the axial plane of the isoclinal folds, with rotated hinges that produce sheath folds having axial planes sub-parallel to L_1 (Carmignani et al., 1993).

The D2 deformation phase was mainly an extensional ductile event that led to isostatic re-equilibration and progressive unroofing and exhumation of the metamorphic units (Carmignani and Kligfield, 1990). The structures of the D1 phase are overprinted by different generations of shear zones and folds with a generally low-dipping to sub-horizontal S_2 schistosity (Carmignani and Giglia, 1975, 1977; Pertusati et al., 1977; Carmignani et al., 1991). According to Carmignani et al. (1978), Carmignani and Giglia (1979) and Carmignani and Kligfield (1990), extension of the metamorphic complex generated a complex mega-antiform with an Apennine-trending axis (NW–SE). Non-cylindrical parasitic folds characterized by sub-horizontal axial planes with transport direction to the E and W were identified respectively on the eastern and western limbs of the antiform. During the final stages of the D2 phase, ductile deformation was replaced by the development of brittle structures (low- and high-angle faults and joint systems) contemporary with the final exhumation and uplift of the metamorphic units in the framework of the late- to post-orogenic regional extension of the inner portion of the Northern Apennines (Ottria and Molli, 2000; Molli et al., 2010).

In this geological context (Fig. 2), the monitored marble quarry is located in the normal limb of the "Pianza anticline" that, together with the "Vallini syncline", represents an antiform-synform pair with core of Jurassic marbles and cherty meta-limenstone. They are minor folds (hectometre-scale) between two D1 structures known as "Carrara syncline" and "Vinca anticline" located to the NW and SE, respectively (Molli and Meccheri, 2012).

Most of the quarried marble belongs to the *White Marble* Group, characterized by homogeneous marbles of medium-fine grain size (about 100-200 µm) and colours ranging from white to ivory-white and from pearl-white to light grey (*Ente Regionale Toscano di Assistenza Tecnica e Gestionale* - ERTAG, 1980). Also present in the quarry is *Ordinary Marble* (Meccheri, 1996), with a medium grain size (about 200 µm) and colours ranging from pearl-white to light grey. Microcrystalline pyrite may form centimetric grey spots and rare light- to dark-grey irregular veins.

Two other subordinate types of marble in the quarry are *Veined Grey Marble* and *Breached Marble* (Carmignani et al., 2007).

The quarry area is characterized by a typical Mediterranean climate with hot, dry summers and cold, wet winters. Precipitation is abundant (over 3000 mm yr^{-1}) with a primary rainfall peak in autumn and two secondary peaks in winter and spring (D'Amato Avanzi et al., 2004). During winter, severe cold waves can drive temperatures to –20°C (Sassolini, 2012).

3. Methods

3.1 Engineering geological surveys

Engineering geological surveys were carried out to characterize the geomechanical properties of discontinuities. The first survey was carried out in accessible areas using traditional scan-line mapping techniques. About 100 discontinuities more than 10 m in length were identified in seven scan lines. Collected data were compared with those by Profeti and Cella (2010) for the same area and integrated with DTP and TLS data in inaccessible zones (Salvini et al., 2014b). The attitude of 301 joints was calculated manually by creating patches that best fit the identified discontinuity planes in the point cloud produced from TLS and extracting their orientation using the Leica™ Cyclone software. In addition, a total of 236 discontinuities were manually identified from stereoscopic photos from an unmanned aerial vehicle (UAV). DTP analysis within the StereoAnalyst module of ERDAS™ IMAGINE allowed us to identify joints and to represent them by coplanar triangles whose attitudes were calculated using spatial analysis techniques (Salvini et al., 2013).

On the basis of engineering geological surveys and data from ERTAG (1980), a kinematic stability analysis of the buttress was carried out using the Markland test (Markland, 1972). Testing was undertaken in order to identify potential failures and the most suitable sensor positions for the geotechnical and RTS monitoring systems. The tests for planar sliding, wedge sliding, and direct toppling were conducted for every accessible face of the buttress, in particular:

1) Southern side of the buttress – strike/dip N80°SE/80°;

2) Eastern side of the buttress – strike/dip N170°E/vertical;

3) Western side of the buttress – strike/dip N160°E/vertical.

3.2 Monitoring systems

3.2.1 Geotechnical system

The geotechnical monitoring system was the first installed on the buttress and it has been run by "*Cooperativa Cavatori Lorano*" and USL1 of Massa and Carrara. It consists of four multipoint borehole extensometers (three bases, the deepest of which is placed at a depth of 30 m), 12 monoaxial mechanical crackmeters, one three-directional crackmeter, and two biaxial clinometers (examples are shown in Fig. 3). The technical specifications of the sensors indicate that the accuracy of monoaxial crackmeters and of extensometers measuring either up to 25 or 50 mm range, is respectively 0.025 and 0.05 mm. The three-directional crackmeter can measure displacements of up to 50 mm and has a resolution of 0.1 mm, with a specified precision better than 0.5% of full scale, corresponding to 0.25 mm. Clinometers have a resolution of 0.001% of the full scale, with a declared precision better than ±0.04°. The data are registered by an electronic control unit every 2 hours. This system has been operative since July 27, 2012, providing high temporal frequency deformation trends to be compared with seasonal variations in the climatological data (rainfall and temperature).

3.2.2 Topographic systems

As specified earlier, the topographic monitoring system consists of an RTS and a ground-based InSAR. Results from the latter are not reported in this paper since, up to now, it was operative for only 6 months and overlapped with other monitoring systems in November 2012 alone. The RTS monitoring system consists of a Leica™ TCA2003 instrument placed approximately 300 m from the buttress, protected by a metallic cage with anti-aberration glasses. This system was employed because it allows the automatic measurement of angles in both azimuth and zenith directions using an electronic theodolite, and distances of visible prisms through a laser infrared distancemeter. Data are collected and sent to a remote PC through an ADSL telephone line. Software packages (GeoMoS Monitor from Leica™, Analysis from Geodesia™, and System Anywhere from Geodesia™) subsequently process the data and produce instantaneous time-displacement graphs. The instrument complies with ISO-17123 and the maximum range is about 1,000 m. The declared range accuracy (RA) is ± 0.5 mm up to 100 m, while for longer distance RA is approximately ± 1 mm plus 1 ppm/Km (parts per million per Km).

The instrumental angular accuracy (AA) of TCA2003 is 0.000135° and complies with DIN-18723. The accuracy of the reading at each prism is dependent on the slope distance from the RTS and is calculated as follows:

$$AA = \tan 0.000135° * \textit{slope distance} \quad (1)$$

Total accuracy (TA) at each prism =

$$\sqrt{RA^2 + {AA_{azimuth}}^2 + {AA_{zenith}}^2} \quad (2)$$

The positioning of the prisms on the buttress took into account findings from the engineering geological surveys and the location of the geotechnical sensors. The RTS is installed in an external stable site (Fig. 4) and automatically takes measurements of 24 prisms fixed to the rock mass by spit anchors. Twenty prisms were placed on the buttress (approximately 300 m from the RTS), most of them located near the geotechnical instruments (Fig. 5), at the hanging wall and footwall of the main discontinuities. Four additional prisms serving as reference points were placed in stable external areas, at a distance ranging from 30 to 430 m.

The selection of the four reference points was critical to obtain accurate results. A thorough geomorphological and structural study was therefore carried out to identify suitable reference point locations. Such points are required to discern relative and absolute displacements; without them, and without proper system calibration, the reliability of results is compromised. Table 1 summarizes the expected accuracy for each prism and its slope distance from the RTS.

Measurement cycles are performed every day at 0:00, 06:00, 12:00 and 18:00 hours. Multiple measurements are taken at every point in order to have a qualitative control of standard deviations. The stability of the RTS was verified during the first few months of data collection through statistical analysis. This enabled processing of multi-temporal data based only on the geometric factors of orientation and scale. The described configuration of the RTS monitoring system, together with the geotechnical one, allowed daily control of the behavior of the buttress and the acquisition of sufficient data.

All 24 prisms were georeferenced in absolute coordinates (UTM-WGS84 Zone 32N) using a differential GPS survey. GPS observations with a static measurement of more than 3 hours were post-processed using differential methods and records from the two nearest permanent GPS stations (La Spezia and Lucca). The orthometric height was calculated in collaboration with the Italian Military Geographic Institute. Consequently the RTS position was calculated with an accuracy of about 1.0 cm. Because the position of the RTS has remained stable since the system became operative (November 26, 2012), measurements of the prisms and their possible displacements are referred to these coordinates. After a literature review (Lavine et al., 2003; Giordan et al., 2013) and other RTS references, the slope distance parameter was selected to illustrate the obtained results. This parameter presents two major advantages over the others: it can be interpreted intuitively and is theoretically accurate because angular measurements are not included.

4. Results

4.1 Joint characterization

Data processing highlighted the following four sets of discontinuities describing the current state of the buttress (Fig. 6): S1 – SW dipping with average dip of about 50°; K1 – SE dipping, sub-vertical; K2 – NE dipping with average dip of about 50°; and K3 – SW dipping, sub-vertical.

The K1, K2, and K3 systems are characterized by metric spacing, millimetric to centimetric apertures, moderate roughness and no infill (Salvini et al., 2014b). According to the Rock Mass Rating (*RMR* – Bieniawski, 1989) the rock mass is of good quality (basic *RMR* or RMR_b = 76).

The identified joint systems can be related to the deformational history of the area. The S1 system, for example, is clearly linked to an axial plane schistosity (S_1), resulting from D1 phase ductile deformation. The K1, K2, and K3 discontinuity systems, instead, are linked to the late stage of the D2 event characterized by the development of brittle structures.

According to Carmignani et al. (2002), the Carrara marble district is characterized by three main systems of discontinuity. The first system, corresponding to K3 of the present study, is often pervasive and almost parallel to S_1; it ranges in direction from N120°E to N150°E and dips steeply to the SW. The second system, corresponding to K1, shows an average anti-Apennine direction ranging from N20–30°E to N80–90°E and a general vertical inclination or sub-vertical (dipping up to 50–60° both to the NW and the SE). The third system, corresponding to K2 of the present study, shows a direction similar to K3 but with a medium-high dip generally to the E and NE.

Ottria and Molli (2000) describe how the mentioned discontinuities can locally evolve into faults with moderated offset. Their paper confirms the complexity of the geological setting, describing a polyphased brittle evolution with two main stages of deformation, DS1 and DS2. The DS1 event was mainly responsible for the development of strike-slip and normal faults related to tensors with horizontal E–W σ3 axes, and σ1/σ2 axes permutations due to trans-extensional tectonics. This is congruent with striae (azimuth/plunge 350°/70°) identified by the authors on an important K3 fracture surface of the quarry wall. The DS2 event may be related to an extensional stress regime characterized by poorly constrained σ3 axes; this event produced NE–SW trending normal faults, in agreement with striae (azimuth/plunge 220°/55°) on a K1 discontinuity in the quarry wall. Ottria and Molli (2000) constrained the timing of DS1 and DS2 phase brittle fracturing to between the Late Pliocene and the Middle Pleistocene, during the final stages of the Apuan uplift.

4.2 Kinematic stability analysis

A discontinuity friction angle of 35° was used in the analysis neglecting a cohesion contribution: this agrees with data in the literature (Chang et al., 1996, Perazzelli et al., 2009) and previous studies carried out by quarry's advisors (Profeti and Cella, 2010). Table 2 shows the potential failures identified through kinematic stability analysis (examples are shown in Fig. 7).

The installation of the monitoring systems was based on results from the kinematic stability analysis. The dynamic analysis of forces and the computation of the safety factors is described in Salvini et al. (2014a).

4.3 Geotechnical monitoring system

To date (March 2014), the analysis of data from the geotechnical monitoring system has revealed no critical situations on the buttress. Fig. 8 shows, as an example, the trends relative to base 1 of extensometer 4 (ES4) and crackmeter 4 (FS4), with maximum displacement values from −0.5 to +1.5 mm.

Although the limited displacements confirm the general stability of the monitored sites, there is a general sinusoidal trend that may be attributed to thermal expansion in summer. Crackmeter data clearly indicate that thermal expansion tends to close fractures while the extensometer data from about 10 m deep show that expansion in winter due to water and ice within fractures is greater than that in summer.

4.4 Topographic monitoring system

Figs. 9 to 12 illustrate the data acquired by the RTS from December 2012 to February 2014. Even in this case, although instrumental accuracy is lower than that of the geotechnical system because of the measurement range, there is a sinusoidal trend similar to the one discussed above. For example, Fig. 9 highlights the correlation between P4 prism displacements and temperature variations, confirming the high thermal susceptibility of the external face of the rock mass. In the summer of 2013, average temperatures reached 27°C with a peak up to 38°C (MeteoApuane, 2015); such high temperatures reduced the slope distance between the RTS and prisms. At the beginning of the cold season there is a change of inflection due to the gradual movement of prisms away from the RTS. In addition to the general trend, the figures show numerous anomalous displacement peaks towards the RTS that in some cases exceed instrumental tolerance. In this case, there is a direct correlation between major rainfall events and peaks registered by the RTS (e.g., Fig. 10). This phenomenon concerns all the prisms installed on the buttress and likely affects the entire rock mass. The displacement of prisms generally appears 1–2 days after rainfall and disappears in as many days without leaving residuals.

The presence of such anomalous peaks, which can reach up to 2 mm, was observed during both the first and second cold seasons. In contrast, no similar anomalies were recorded during the only warm season analysed to date (summer of 2013). Note that none of the reference prisms installed outside the buttress (neither the closest, R2, nor the farthest, R4, approximately 30 m and 430 m respectively from the RTS - Fig.11) show such anomalous displacements. Furthermore, doing the dynamic analysis using all the prisms but with none assigned as reference points, does not change the trend of displacement of processed prisms.

Fig. 12 shows a comparison between the diagram of prism G19 and the extensometer ES4, whose deepest base (base 3) is located 30 m inside the slope, and ES3 (base 1) in the buttress.

4.4.1 Displacement vectors

In order to verify the displacement entity and direction of each prism, the absolute coordinates of the prisms on different dates were converted to vectors. Fig. 13 shows the displacement vectors and relative error ellipses for the period December 2012 – December 2013. The final coordinates of prisms are calculated as an average of 10-day measurements to avoid anomalous daily responses due to rain, haze, etc.; ellipses were calculated based on instrumental tolerance and prism distances from the RTS (see Table 1 for details).

The annual displacement vectors indicate that the behavior of the rock mass may not be completely elastic. The moduli vary between 2 and 3 mm, with peaks of 6–7 mm for prisms P8, G13 and G19, and have S–SW directions of displacement. Only three out of 20 prisms (G20, G18 and P10) diverge considerably from this direction. This difference can be explained by local multi-directional movements caused by fracturing. However, note that the moduli of the latter three vectors do not exceed instrumental tolerances and are therefore considered unreliable. The displacement directions of all other prisms are often concordant and the moduli often exceed instrumental accuracy.

The analysis of the prism movement after a single rainfall event confirms that displacement vectors for the maximum peak have an S–SW direction. For example, Fig. 14 shows the displacement vectors for three prisms (P4, G14 and G20). The same direction of movement is then confirmed also after single rainfall events, without exceeding instrumental tolerances.

5. Discussion

The results of the present paper highlight two main aspects: the response of the buttress to the temperature variations and the rainfall events, and the entity and direction of prisms displacement vectors. The trend wave recorded by all the analysed monitoring systems, related to temperature variations, can be associated with the properties of marble subject to thermoclasty, whose behavior can be linked to the contraction or elongation of calcite determined by crystallographic axes (Siegesmund et al., 2000; Malaga-Starzec et al., 2002). Different climate conditions may affect diversely the response of some prisms; for example, winter 2013 – 2014 was characterized by average temperatures about 2°C higher than the previous year and some prisms showed residual displacement at the end of the analysed period (e,g., Figs. 9, 10, and 12). Nevertheless, further studies covering more seasonal cycles are necessary to verify whether the behavior of the rock mass is elastic or inelastic.

Concerning the anomalous peaks of displacement during major rainfall events, the influence of atmospheric conditions on RTS measurements has already been addressed in the literature. Afeni and Cawood (2013) illustrate how rainfall events combined with low visibility due to haze can lead to errors in measurement. In the present study, however, the anomalous measurements persist several hours to 2 days after the rainfall and in sunny weather. Moreover, the absence of anomalous peaks in the charts of reference prisms reasonably excludes errors due to adverse atmospheric conditions. Nevertheless, the differences between the diagrams for prisms measured by the RTS and the geotechnical sensors in the same area lead to two considerations. First, the registered peaks of displacement could be linked to the overall behavior of the structure, irrespective of individual discontinuities; only the RTS can record this behavior because of the availability of data from the four reference prisms outside the buttress and the slope. Second, water may infiltrate deep in the mountain and neither the deepest extensometer ES4 in the slope, nor ES3 in the buttress, can register it entirety. The geotechnical sensors may record only relative movements, not absolute displacements, because they move integrally with the buttress. Therefore, data processing in relation to the four stable external reference points was essential.

Sensitivity to rainfall events may be due to a set of NE–SW trending pseudo-vertical discontinuities intersecting the rock mass on top of and at the back of the buttress (Fig. 15). During relevant rainfall events, water infiltrated in discontinuities can cause a pressure that may dilate joints. Note that recovery after rainfall appears to be elastic, although a longer series of data is needed to adequately investigate this.

We hypothesize that the observed S–SW displacement recorded by the prisms on the buttress can be connected to a stress field favored by the jointed morphology of the back slope of the buttress, detensioning due to ongoing excavation activity, and extensional stresses toward SW due to the geological uplift of the entire Apuan core complex (Ottria and Molli, 2010). Despite the short monitoring period to discuss the elastic/inelastic behavior of the rock mass, newly formed brittle fractures on the buttress support the above inference. Fig. 16 shows an example of brittle fractures at the toe of the buttress. The attitude of the newly formed fractures (Dip Direction/Dip 19°/85° – K4 in Salvini et al., 2014b) agrees with the presumed tensional stress field. However, this consideration is still hypothetical and it has to be confirmed by in-situ stress measurements in the future.

6. Conclusions

Safety in quarries and the risk of slope instability is a complex matter, especially in a dynamic environment where anthropogenic perturbations may induce geomorphological hazards. In a quarry, an adequate monitoring system is very important for preventing such hazards. The monitoring system installed at the "Lorano" marble quarry is an example of a modern, integrated system comprising traditional geotechnical instruments, a robotic total station and, for a brief period, a terrestrial interferometer. The identification of the location and type of slope instability is important, therefore we conducted engineering geological surveys, photointerpretation of UAV images and kinematic stability analyses.

This research demonstrates a fourteen month analysis of system data and findings. A longer period of time must elapse and in situ stress measurements must be made to gain a more complete understanding of the behavior of the buttress under study. To date, findings indicate that the slope is generally stable, no rock fall has occurred, and that safety limits have never been exceeded, not even in the few potentially critical areas. However, data highlighted a general sinusoidal trend possibly linked to structural responses to seasonal temperature variations. The robotic total station also recorded an elastic response of the buttress after major rainfall events although the geotechnical sensors did not detect this because they are only sensitive to relative movements, not the absolute displacements of the entire structure. The absence of anomalous responses of the geotechnical sensors after the major rainfall events indicates that the recorded displacements are not linked to water circulation within minor fractures in the pillar. Although the geotechnical monitoring system has a higher accuracy, only the RTS system provides a complete picture of the buttress deformation. Therefore, the use of external reference prisms turned out to be appropriate; they were used to exclude errors due to atmospheric interference and to assess the displacements of the buttress that would otherwise have been undetected without very deep borehole extensometers. The direction of prism displacement both during the entire investigated period and after intense rainfalls, as well as the presence of newly formed brittle fractures, suggests a tensional stress field with NE–SW extension. These observations confirm the importance of integrating different monitoring systems to provide indications at different spatial scales.

Acknowledgments

The present study was undertaken within the framework of the Italian National Research Project PRIN2009, funded by the Ministry of Education, Universities and Research, which involves the collaboration between the University of Siena, "La Sapienza" University of Rome, and USL1 of Massa and Carrara (Mining Engineering Operative Unit – Department of Prevention).

The authors also acknowledge Pellegri, M. (USL1); Ferrari, M., Profeti, M., Carnicelli, V. (Cooperativa Cavatori Lorano); and Bozzano, F., Mazzanti, P., Rocca, A. ("La Sapienza" University of Rome) for their support of this research.

References

Afeni, T.B., Cawood, F.T., 2013. Slope monitoring using total station: What are the challenges and how should these be mitigated. S. Afr. J. Geomat. 2, 41-53.

Aryal, A., 2013. Landslide deformation character inferred from terrestrial laser scanner data. PhD Thesis, University of Hawaii at Manoa, pp. 97.

Bieniawski, Z.T., 1989. Engineering rock mass classifications. John Wiley and Sons, New York.

Boccaletti, M., Elter, P., Guazzone, G., 1971. Plate tectonic models for the development of the Western Alps and Northern Apennines. Nature 234, 108-111.

Carmignani, L., Giglia, G., 1975. Le fasi tettoniche terziarie dell'Autoctono delle Alpi Apuane: studio delle strutture minori della zona centro-meridionale. Boll. Soc. Geol. It. 94, 1957-1981.

Carmignani, L., Giglia, G., 1977. Analisi mesostrutturale della zona occidentale delle Apuane metamorfiche. Boll. Soc. Geol. It. 96, 429-450.

Carmignani, L., Giglia, G., 1979. Large scale reverse “drag folds” in the late Alpine building of the Apuane Alps (N. Apennines). Proc. Soc. Tosc. Sci. Nat. 86, 109-126.

Carmignani, L., Kligfield, R., 1990. Crustal extension in the northern Apennines: the transition from compression to extension in the Alpi Apuane Core Complex. Tectonics 9, 1275-1303.

Carmignani, L., Giglia, G., Kligfield, R., 1978. Structural evolution of the Apuane Alps; an example of continental margin deformation in the northern Apennines, Italy. J. Geol. 86, 487-504.

Carmignani, L., Giglia, G., Kligfield, R., 1980. Nuovi dati sulla zona di taglio ensialica delle Alpi Apuane. Mem. Soc. Geol. It. 21, 93-100.

Carmignani, L., Fantozzi, P.L., Meccheri, M., 1991. La vergenza "sin" e "post-nappe" della Falda Toscana nelle strutture di Pescaglia e di Castelpoggio. Boll. Soc. Geol. It. 110, 351-364.

Carmignani, L., Disperati, L., Fantozzi, P.L., Giglia, G., Meccheri, M., 1993. Tettonica distensiva del complesso metamorfico delle alpi apuane -Guida all’escursione-. Siena, pp. 128.

Carmignani, L., Antompaoli, L., Appelius, V., Bocci, M., Chiereghin, F., Coli, M., Fantozzi, P.L., Frosini, S., Grazioni, B., Livi, V., Mariottini, E., Meccheri, M., Piccini, L., Pini, G., Rossi, L.M., Sciuto, P.F., 2002. Studi conoscitivi sui bacini marmiferi industriali di Carrara: un contributo per la gestione pianificata dell'attività. GEAM - Geoingegneria Ambientale e Mineraria, Torino, pp. 21-43.

Carmignani, L., Conti, P., Mancini, S., Massa, G., Meccheri, M., Simoncini, D., Vaselli, L., 2007. Carta Giacimentologica dei Marmi delle Alpi Apuane - RELAZIONE FINALE. Technical report, Centre of GeoTechnologies, University of Siena, Italy.

Chang, C.T., Monteiro, P., Nemati, K., Shyu, K., 1996. Behavior of Marble under compression. J. Mater. Civil Eng. 8, 157-170.

Conti, P., Di Pisa, A., Gattiglio, M., Meccheri, M., 1993. Prealpine basement in the Alpi Apuane (Northern Apennines, Italy). In: Von Raumer, J.F., Neubauer, F. (Eds.), Pre-Mesozoic geology in the Alps. Springer Verlag, pp. 609-621.

Conti, P., Carmigani, L., Giglia, G., Meccheri, M., Fantozzi, P. L., 2004. Evolution of geological interpretations in the Alpi Apuane Metamorphic Complex, and their relevance for the geology of the Northern Apennines. In: Morini, D., Bruni, P. (Eds.), The “Regione Toscana” project of geological mapping.Firenze, Italy, pp. 241-262.

D'Amato Avanzi, G., Giannecchini, G., Puccinelli, R., 2004. The influence of the geological and geomorphological settings on shallow landslides. An example in a temperate climate environment: the June 19, 1996 event in northwestern Tuscany (Italy). Eng. Geol. 73, 215-228.

Dercourt, J., Zonenshain, L.P., Ricou, L.E., Kazmin, V.G., Le Pichon, X., Knipper, A.L., Grandjacquet, C., Sbortshikov, I.M., Geyssant, J., Lepvrier, C., Pechersky, D.H., Boulin, J., Sibuet, J.C., Savostin, L.A., Sorokhtin, O., Westphal, M., Bazhenov, M.L., Lauer, J.P., Biju-Duval B., 1986. Geological evolution of the Tethys belt from the Atlantic to the Pamirs since the Lias. Tectonophysics 123, 241-315.

Elter, P., 1975. L'ensemble ligure. Bull. Soc. Geol. France 17, 984-997

ERTAG, 1980. I Marmi Apuani. Nuova Grafica Fiorentina, Firenze.

Fekete, S., Diederichs, M., 2013. Integration of three-dimensional laser scanning with discontinuum modelling for stability analysis of tunnels in blocky rockmasses, Int. J. Rock Mech. Min. 57, 11-23.

Firpo, G., Salvini, R., Francioni, M., Ranjith, P.G., 2011. Use of Digital Terrestrial Photogrammetry in rocky slope stability analysis by Distinct Elements Numerical Methods. Int. J. Rock Mech. Min. 48, 1045-1054.

Gattiglio, M., Meccheri, M., Tongiorgi, M., 1989. Stratigraphic correlation forms of the Tuscan Palaeozoic basement. Rend. Soc. Geol. It. 12, 247-257.

Gigli, G., Fanti, R., Canuti, P., Casagli, N., 2011. Integration of advanced monitoring and numerical modeling techniques for the complete risk scenario analysis of rockslides: The case of Mt. Beni (Florence, Italy). Eng. Geol. 120, 48-59.

Giordan, D., Allasia, P., Manconi, A., Baldo, M., Santangelo, M., Cardinali, M., Corazza, A., Albanese, V., Lollino, G., Guzzetti, F., 2013. Morphological and kinematic evolution of a large earthflow: The Montaguto landslide, southern Italy. Geomorphology 187, 61-79.

Griffiths, J.S., Hutchinson, J.N., Brunsden, D., Petley, D.J. and Fookes, P.G., 2004. The reactivation of a landslide during the construction of the Ok Ma tailings dam, Papua New Guinea. Q. J. Eng. Geol. Hydroge. 37, 173-186.

Kenner, R., Bühler, Y., Delaloye, R., Ginzler, C., Phillips, M., 2014. Monitoring of high alpine mass movements combining laser scanning with digital airborne photogrammetry, Geomorphology 206, 492-504.

Kristensen, L., Rivolta, C., Dehls, J., Blikra, L.H., 2013. GB InSAR measurement at the Åknes rockslide, Norway. In: Genevois R and Prestininzi A. (Eds.), International conference on Vajont – 1963-2013, Book series 6. Ital. j. eng. geol. Environ., Rome, Italy, pp. 339-348.

Kuhlmann, H., Glaser, A., 2002. Investigation of new measurement techniques for bridge monitoring. Proc. 2nd Symp. Geod. Geotech. Struct. Eng. Berlin, Germany, pp 123-132.

Lavine, A., Gardner, J.N., Reneau, S.L., 2003. Total station geologic mapping: an innovative approach to analyzing surface-faulting hazards. Eng. Geol. 70, 71-91.

Liu, D.A., Yang, Z.F., Tang, C.H., Wang, J., Liu, Y., 2004. An automatic monitoring system for the shiplock slope of Wuqiangxi Hydropower Station. Eng. Geol. 76, 79-91.

Malaga-Starzec, K., Lindqvist, J. Schouenburg, B., 2002. Experimental study on the variation in porosity of marble as a function of temperature. J. Geol. Soc. London 205, 81-88.

Markland, J.T., 1972. A useful technique for estimating the stability of rock slopes when the rigid wedge slide type of failure is expected. Imperial College Rock Mechanics Research Reprints, n. 19.

Marroni, M., Meneghini, F., Pandolfi, L., 2010. Anatomy of the Ligure - Piemontese subduction system: evidence from Late Cretaceous, Middle Eocene convergent margin deposits in The Northern Apennines, Italy. Int. Geol. Revi. 2, 1-33.

Meccheri, M., 1996. Carta Geologico – Strutturale delle varietà merceologiche dei Marmi del Carrarese. Scala 1:10.000. Dipartimento di Scienze della Terra, Siena Univ.

MeteoApuane, 2015. Associazione “Meteo Apuane”, http://www.meteoapuane.it (access date March 01, 2015)”

Molli, G., 2008. Northern Appennine-Corsica orogenic system: an updated review. In: S. Siegesmund, B. Fügenschuh, and N. Froidzheim (Eds.), Tectonic Aspects of the Alpine-Dinaride-Carpathian System. J. Geol. Soc. London Special Publication 298, 413-442.

Molli, G., Meccheri, M., 2012. Structural inheritance and style of reactivation at mid-crustal levels: A case study from the Alpi Apuane (Tuscany, Italy). Tectonophysics 579, 74-87.

Molli, G., Cortecci, G., Vaselli, L., Ottria, G., Cortopassi, A., Dinelli, E., Mussi, M., Barbieri, M., 2010. Fault zone structure and fluid-rock interaction of a high angle normal fault in Carrara marble (NW Tuscany, Italy). J. Struct. Geol. 32, 1334-1348.

Ottria, G., Molli, G., 2000. Superimposed brittle structures in the late orogenic extension of the northern Apennine: results from Carrara area (Alpi Apuane, NW Tuscany). Terra Nova 12, 1-8.

Pankow, K.L., Moore, J.R., Hale, J.M., Koper, K.D. Kubacki, T., Whidden, K.M., McCarter, M.K., 2014. Massive landslide at Utah copper mine generates wealth of geophysical data. GSA Today, 24, 4-9.

Perazzelli, P., Rotonda, T., Graziani, A., 2009. Stability analysis of an active marble quarry by DEM modelling. Proc. Int. Conf. Rock. Joints & Jointed Rock Masses, Tucson, Arizona, USA.

Pertusati, P.C., Plesi, G., Cerrina Feroni, A., 1977. Alcuni esempi di tettonica polifasata nella Falda Toscana. Boll. Soc. Geol. It. 96, 587-603.

Profeti, M., 2013. Relazione tecnica sul monitoraggio strumentale. Tecnichal report, Coop Cavatori Lorano.

Profeti, M., Cella, R., 2010. Relazione sulla stabilità dei fronti. Tecnichal report, Coop Cavatori Lorano.

Robbins, J.C., Petterson, M.G., Mylne, K., and Espi, J.O., 2013. Tumbi landslide, Papua New Guinea: rainfall induced?. Landslides 10, 673-684.

Salvini, R., Francioni, M., Riccucci, S., Bonciani, F., Callegari, I., 2013. Photogrammetry and laser scanning for analyzing slope stability and rock fall runout along the Domodossola–Iselle railway, the Italian Alps. Geomorphology 185, 110-122.

Salvini, R., Riccucci, S., Gullì, D., Giovannini, R., Vanneschi, C., Francioni, M. 2014a. Geological application of UAV photogrammetry and terrestrial laser scanning in marble quarrying (Apuan Alps, Italy). In: Lollino, G., Manconi, A., Guzzetti, F., Culshaw, M., Bobrowsky, P., Luino, F. (Eds.), Engineering Geology for Society and Territory -Volume 5. Springer, pp 979-983.

Salvini, R., Giovannini, R., Vanneschi, C., Francioni, M., Stead, D., Riccucci, S., Gullì, D., 2014b. The use of remote sensing for discontinuity mapping and analysis in a large marble quarry, Carrara, Italy. I Int. Conf. Discrete Fracture Network Engineering, Vancouver, British Columbia, Canada.

Salvini, R., Riccucci, S., Gullì, D., Giovannini, R., Vanneschi, C., Francioni, M., 2014c. Integration of geotechnical and remote monitoring systems for the analysis and control of ground deformation in marble quarrying (Apuan Alps, Italy). In: Lollino, G., Manconi, A., Guzzetti, F., Culshaw, M., Bobrowsky, P., Luino, F. (Eds.), Engineering Geology for Society and Territory -Volume 5. Springer, pp 183-187.

Sarwar, G.M., 2008. Landslide Tragedy of Bangladesh. The First World Landslide Forum, United Nations University, Tokyo, Japan, pp. 513-516.

Sassolini, E., 2012. Il clima dell’Italia. http://www.centrometeoitaliano.it/notizie-meteo/il-clima-dell-italia/ (access date March 01, 2015).

Scandone, P., 1979. Origin of the Tyrrhenian Sea and Calabrian Arc. Boll. Soc. Geol. It. 98, 27-34.

Schulz, W.H., Coe, J.A., Shurtleff, B.L., Panosky, J., Farina, P., Ricci, P.P., Barsacchi, G., 2012. Kinematics of the Slumgullion landslide revealed by ground-based InSAR surveys. In: Eberhardt et al. (Eds.), Landslides and Engineered Slopes: Protecting Society through Improved Understanding. CRC Press, Banff, Canada, pp. 1273-1279.

Semenza, E., 1965. Sintesi degli studi geologici sulla frana del Vajont dal 1959 al 1964. Memorie del Museo Tridentino di Scienze Naturali 16, 1-51.

Siegesmund, S., Ullmeyer, K., Weiss, T. Tschegg E.K., 2000. Physical weathering of marbles caused by anisotropic thermal expansion. Int. J. Earth Sci. 89, 170-82.

Sturzenegger, M., Stead, D., 2009. Close-range terrestrial digital photogrammetry and terrestrial laser scanning for discontinuity characterization on rock cuts. Eng. Geol. 106, 163-182.

Teza, G., Marcato, G., Pasuto, A., Galgaro, A., 2014. Integration of laser scanning and thermal imaging in monitoring optimization and assessment of rockfall hazard: a case history in the Carnic Alps (Northeastern Italy). Nat. Hazards 76, 1535-1549.

Tsai, Z.X., You, G.J.Y., Lee, H.Y., Chiu, Y.J., 2011. Use of a total station to monitor post-failure sediment yields in landslide sites of the Shihmen reservoir watershed, Taiwan. Geomorphology 139-140, 438-451.

Wieczorek, G.F., Snyder, J.B., 2009. Monitoring slope movements. In: Young, R., Norby, L. (Eds.), Geological Monitoring. Soc, Geol. America, Boulder, Colorado, pp. 245-271.

Zaccagna, D., 1932. Descrizione Geologica delle Alpi Apuane. Memorie Descrittive della Carta Geologica d'Italia 25, 1-440.

Tables

Table 1. Range and the expected angular and total accuracy (acc.) of measurement for each prism.

Prism	Slope distance (m)	Range acc. (± mm)	Angular acc. (±°)	Angular acc. (± mm)	Total acc. (± mm)
G1	301	1.20	0.000135	0.72	1.58
G2	305	1.20	0.000135	0.73	1.59
G13	300	1.20	0.000135	0.72	1.58
G14	298	1.20	0.000135	0.72	1.57
G15	295	1.19	0.000135	0.71	1.56
G16	292	1.19	0.000135	0.70	1.55
G17	295	1.19	0.000135	0.71	1.56
G18	294	1.19	0.000135	0.71	1.55
G19	329	1.20	0.000135	0.79	1.64
G20	312	1.20	0.000135	0.75	1.60
P3	290	1.19	0.000135	0.70	1.55
P4	289	1.18	0.000135	0.70	1.54
P5	286	1.18	0.000135	0.69	1.53
P6	285	1.18	0.000135	0.69	1.53
P7	293	1.19	0.000135	0.71	1.55
P8	294	1.19	0.000135	0.71	1.56
P9	282	1.18	0.000135	0.68	1.52
P10	283	1.18	0.000135	0.68	1.52
P11	280	1.18	0.000135	0.68	1.52
P12	282	1.18	0.000135	0.68	1.52
R1	111	1.01	0.000135	0.27	1.08
R2	34	0.54	0.000135	0.08	0.55
R3	320	1.20	0.000135	0.77	1.62
R4	431	1.31	0.000135	1.04	1.97

Table 2. Potentially unstable joint systems along the three different slopes of the buttress.

Buttress side	Planar sliding	Wedge sliding	Direct Toppling
Southern	S1	K1/S1	K1/K3
Eastern	K1 - K2	K1/K2 - K1/K3	-
Western	S1 - K3	K1/K3 - K1/S1	-

Figure captions

Fig. 1. Study area. a) Topography of the site. Black circle indicates the marble buttress; inset map shows the location of the study area (modified from Salvini et al., 2014a). b) Panoramic picture of the quarry with the buttress under study in the foreground.

Fig. 2. Geological sketch map of the Apuan Alps. The black rectangle indicates the location of the quarry (modified from Conti et al., 2004).

Fig. 3. Examples of geotechnical sensors installed on the buttress. a) Monoaxial mechanical crackmeter. b) Biaxial clinometers. c) Three-directional crackmeter. d) Multipoint borehole extensometer (modified from Profeti, 2013).

Fig. 4. UAV orthophoto showing the location of prisms, reference points and the RTS.

Fig. 5. Location of geotechnical sensors and RTS prisms on the western (a), southern and eastern (b) sides of the buttress.

Fig. 6. Joint systems. a) Pole plots and mean attitudes of joint systems from engineering geological, DTP and TLS surveys. Data are shown in stereographic projection using the Schmidt equal-area method (lower hemisphere). b) Examples of K1, K2, and K3 joint systems and S1 schistosity in the buttress.

Fig. 7. Examples of kinematic stability analysis carried out using Dips 6.0 (Rocscience^{TM}), stereographic projection through the Wulff equal-angle method (lower hemisphere). a) Planar sliding on the eastern side of the buttress. b) Wedge sliding on the eastern side of the buttress. c) Direct toppling on the natural slope above the western side of the buttress.

Fig. 8. Time-displacement charts relative to geotechnical sensors: a) ES4 and b) FS4.

Fig. 9. Time series displacement relative to prism P4 (December 2012 – February 2014) vs daily average temperature (MeteoApuane, 2015).

Fig. 10. Time series of displacement relative to prism P5 (December 2012 – February 2014) vs daily average temperature and rainfall (MeteoApuane, 2015).

Fig. 11. Time series of displacements relative to reference prisms (December 2012 – February 2014) vs daily average temperature and rainfall (MeteoApuane, 2015): a) R2 and b) R4.

Fig. 12. Time-displacement diagrams relative to geotechnical sensors ES3 and ES4 (a) and prism G19 (b) (December 2012 – February 2014) vs daily average temperatures and rainfall (MeteoApuane, 2015). Inset map shows an aerial view of the buttress and the location of the three sensors.

Fig. 13. Displacement vectors and error ellipses for the December 2012 – December 2013 period.

Fig. 14. Vectors showing the displacement of three prisms after an important rainfall event (pre-event date January 19, 2013 – post-event date January 21, 2013).

Fig. 15. UAV ortophoto with the main photointerpreted discontinuities; inset picture shows a fault system intersecting the rock mass at the back of the buttress.

Fig. 16. Newly formed set of joints at the toe of the buttress.

Figure 1 (Color) - single-column

Click here to download high resolution image

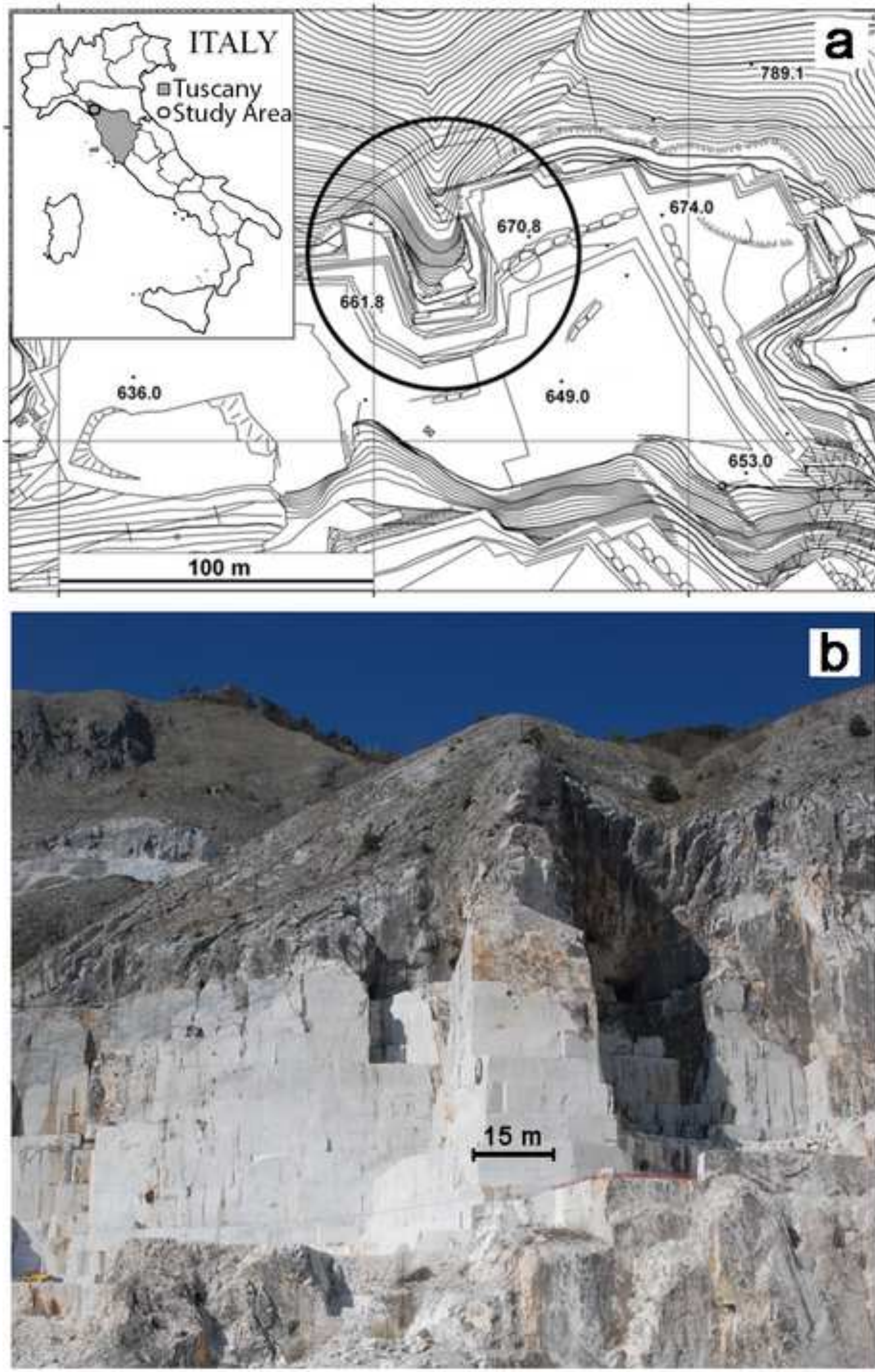

Figure 2 (Color) - 2-column

Click here to download high resolution image

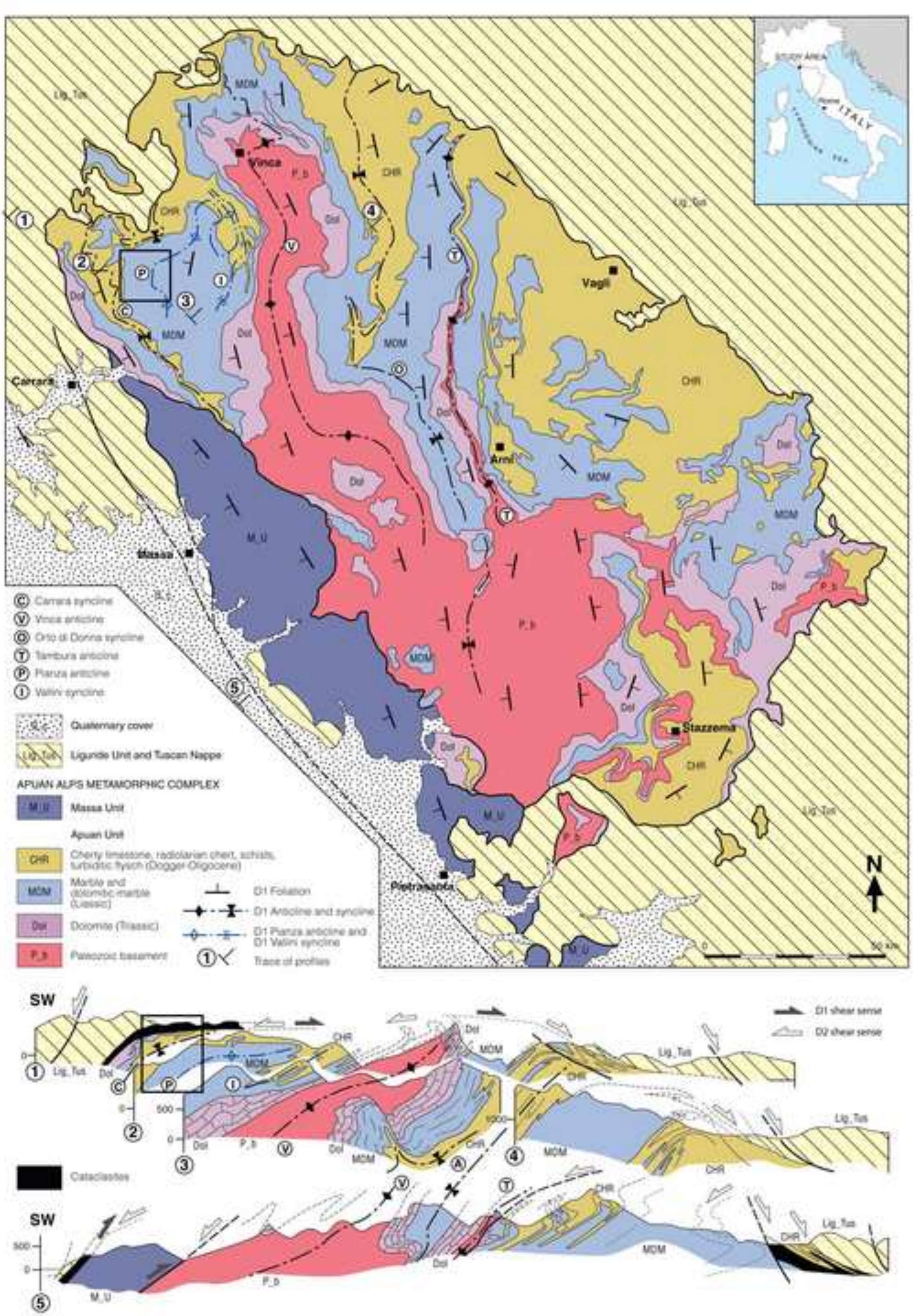

Figure 3 (Color) - single-column

Click here to download high resolution image

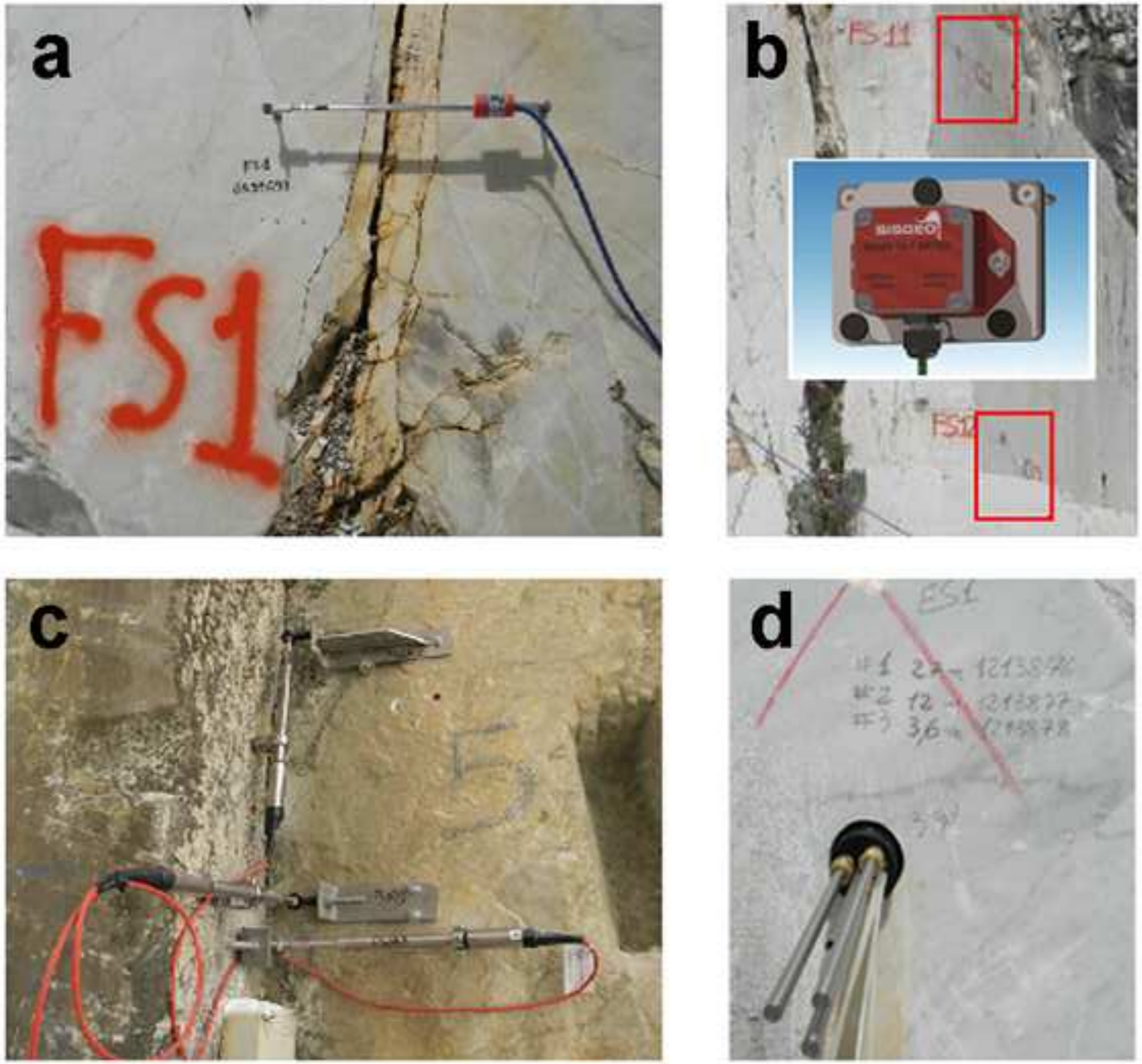

Figure 4 (Color) - 2-column
Click here to download high resolution image

Figure 5 (Color) - 2-column
Click here to download high resolution image

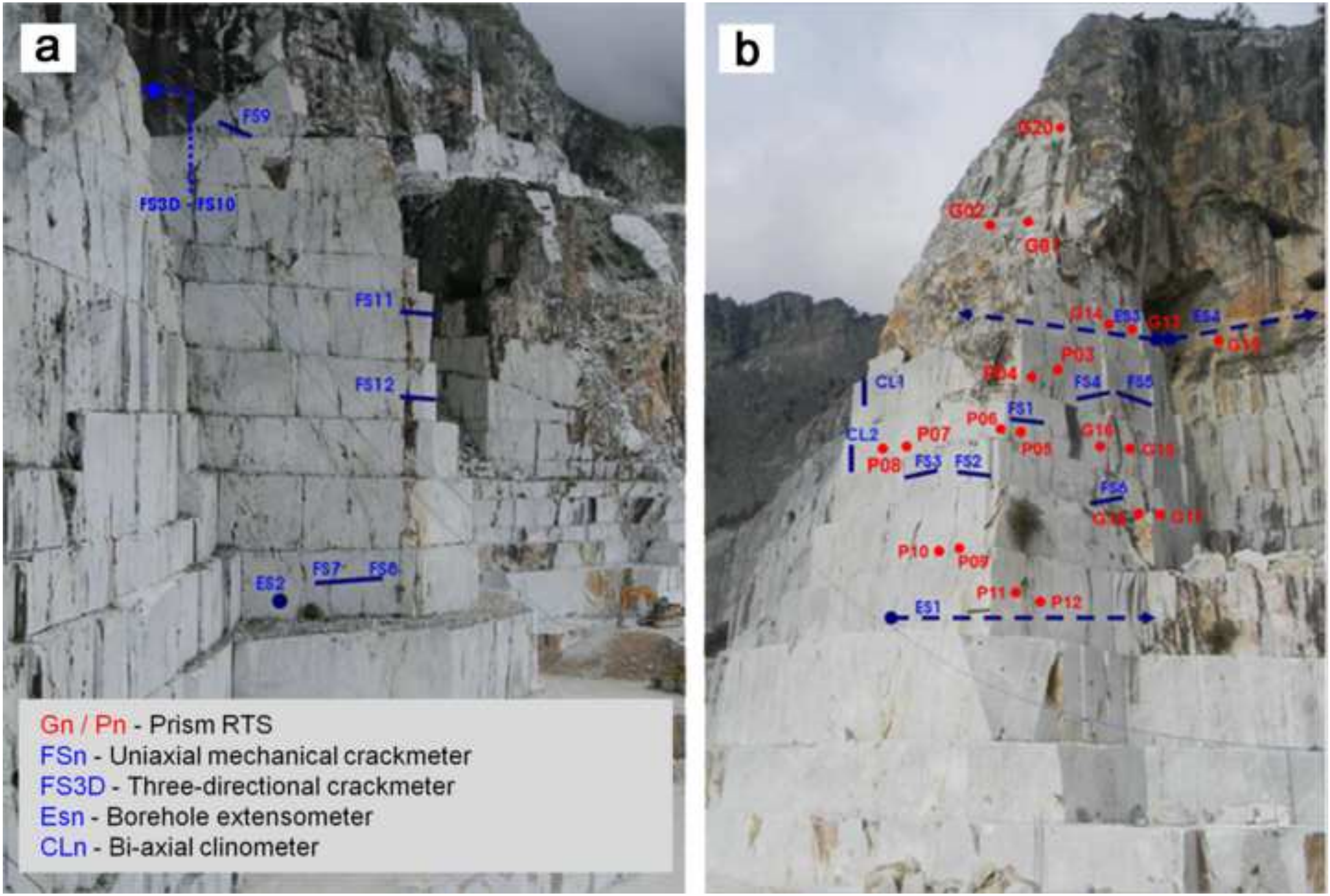

Figure 6 (Color) - 2-column
Click here to download high resolution image

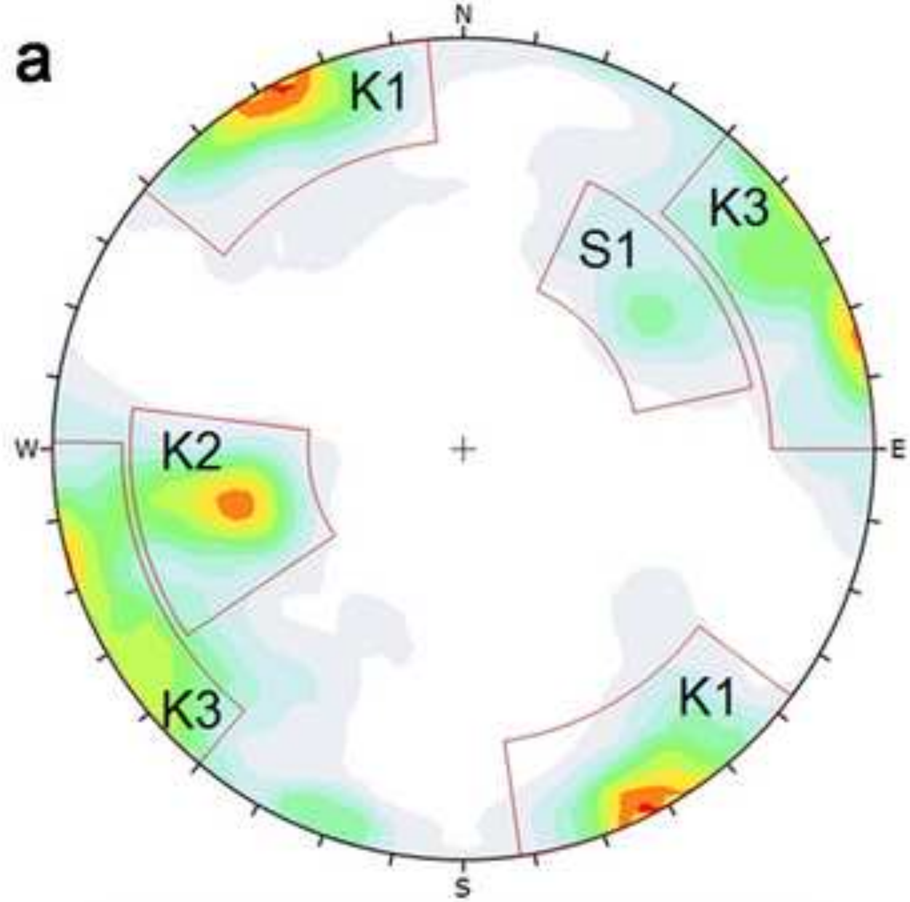

Plot Mode	Pole Vectors
Vector Count	630 (630 Entries)
Hemisphere	Lower
Projection	Equal area

System	Dip (°)	Dip Direction (°)
K1	87	149
K2	50	76
K3	89	244
S1	51	229

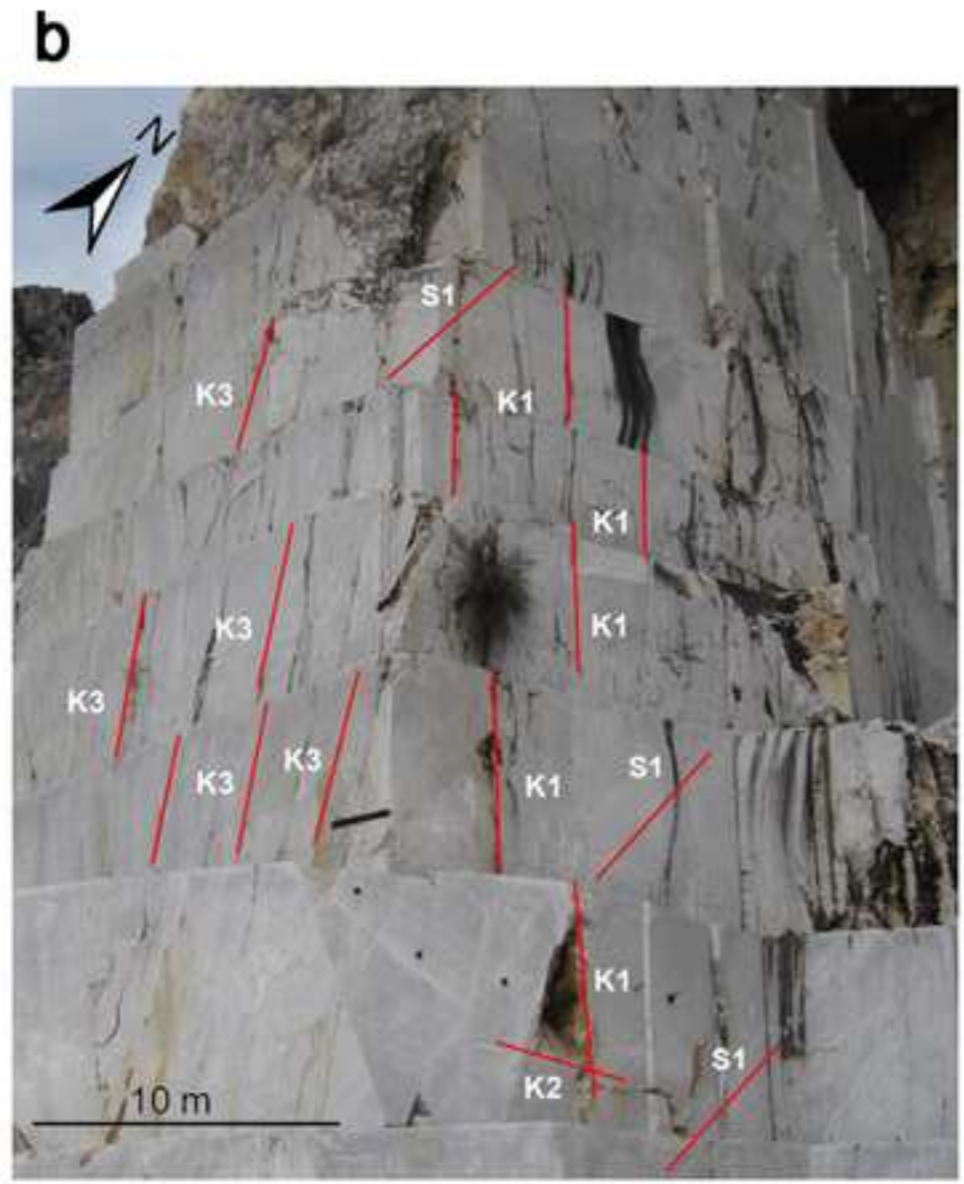

Figure 7 (Color) - 2-column

Click here to download high resolution image

a

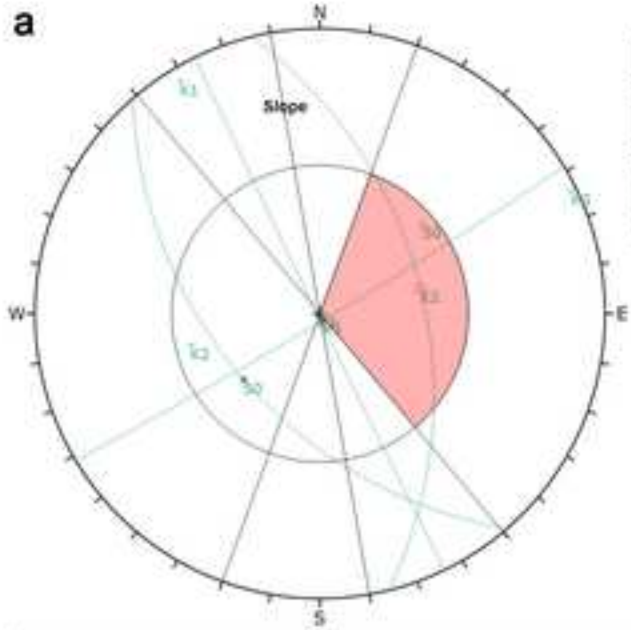

Kinematic Analysis	Planar Sliding
Slope Dip/Dip Direction	90/80
Friction Angle	35°
Lateral Limits	60°

	Critical	Total	%
Planar Sliding (All)	1	4	25

b

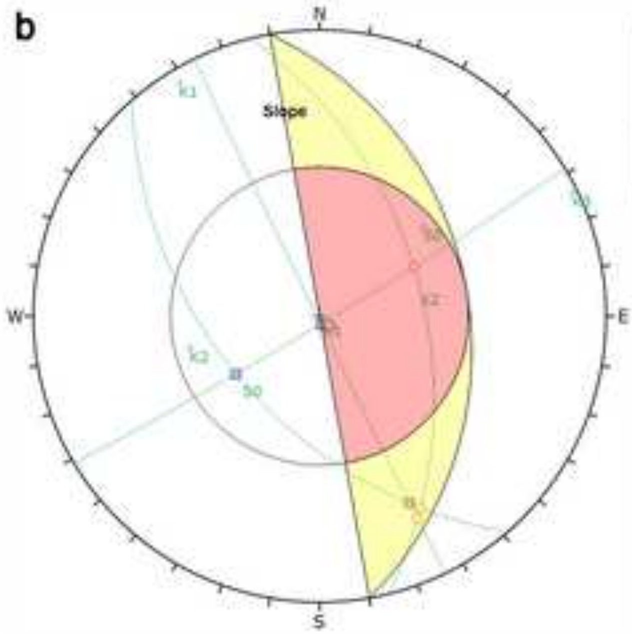

Kinematic Analysis	Wedge Sliding
Slope Dip/Dip Direction	90/80
Friction Angle	35°

	Critical	Total	%
Wedge Sliding	3	6	50

c

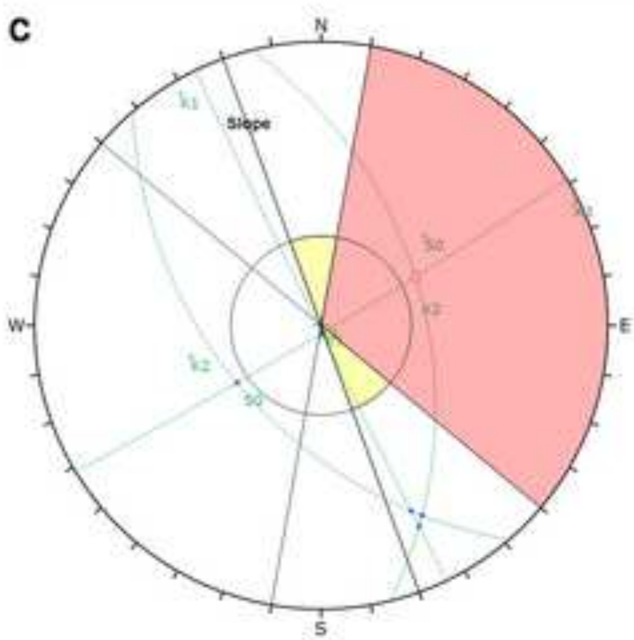

Kinematic Analysis	Direct Toppling
Slope Dip/Dip Direction	90/250
Friction Angle	35°
Lateral Limits	60°

	Critical	Total	%
Direct Toppling (Intersection)	1	6	16.6
Oblique Toppling (Intersection)	0	6	0
Base Plane (All)	2	4	50

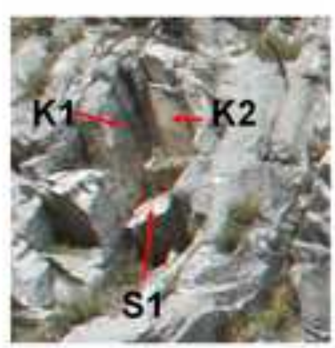

Figure 8 (Color) - 2-column

Click here to download high resolution image

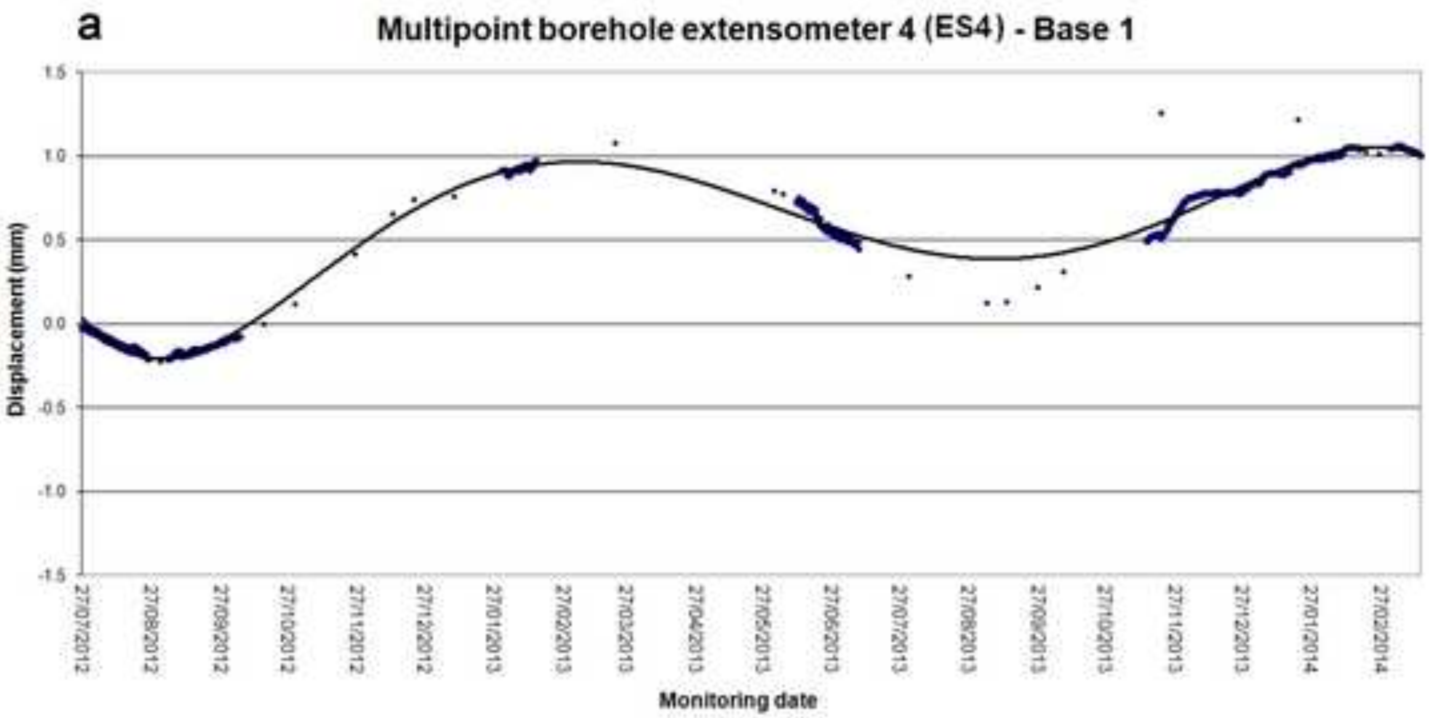

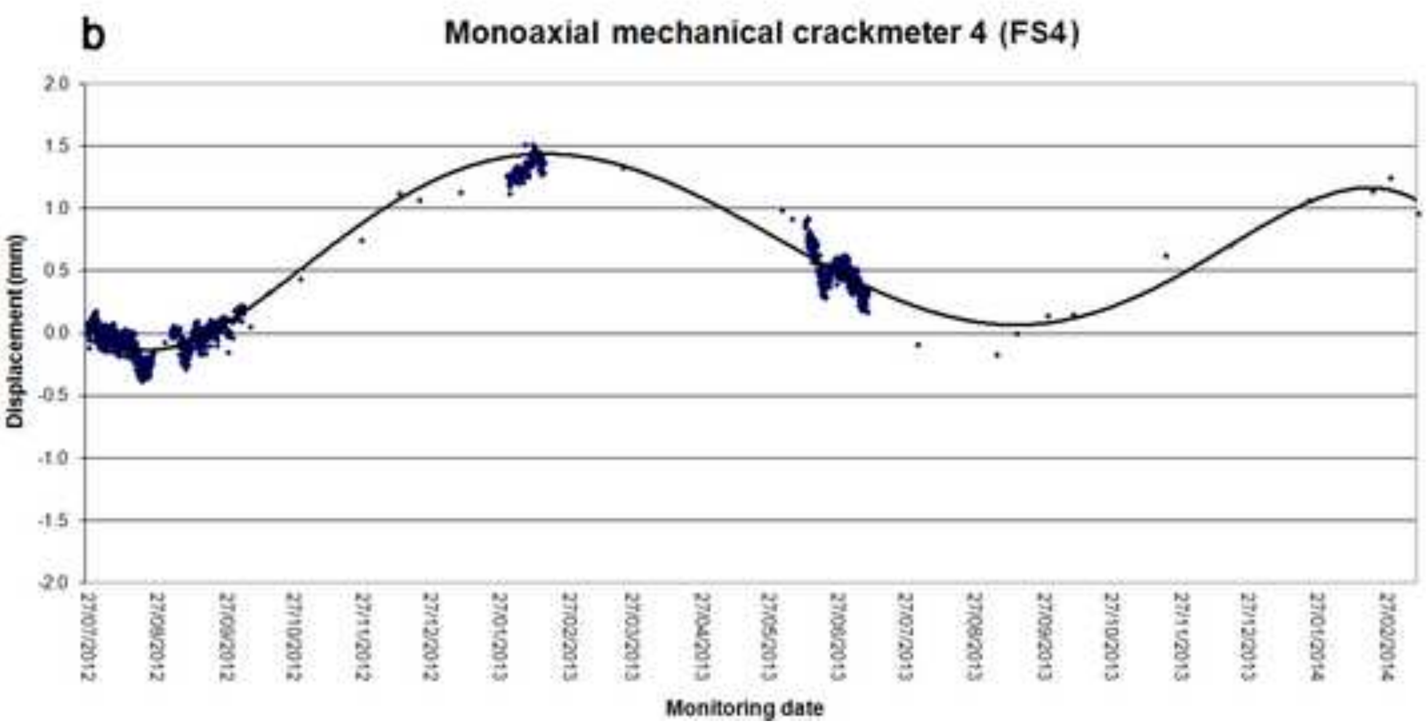

Figure 9 (Color) - 2-column

Click here to download high resolution image

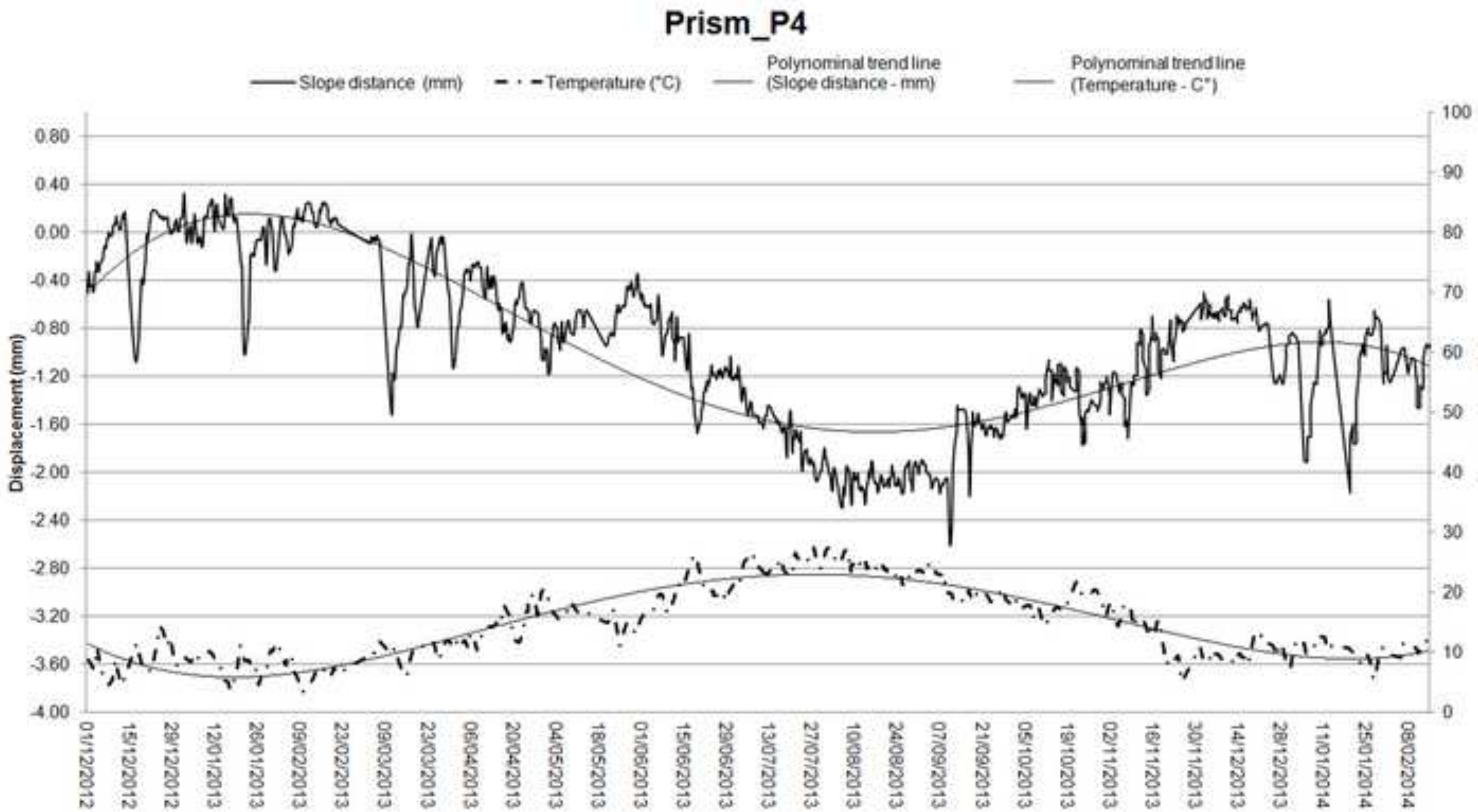

Figure 10 (Color) - 2-column
Click here to download high resolution image

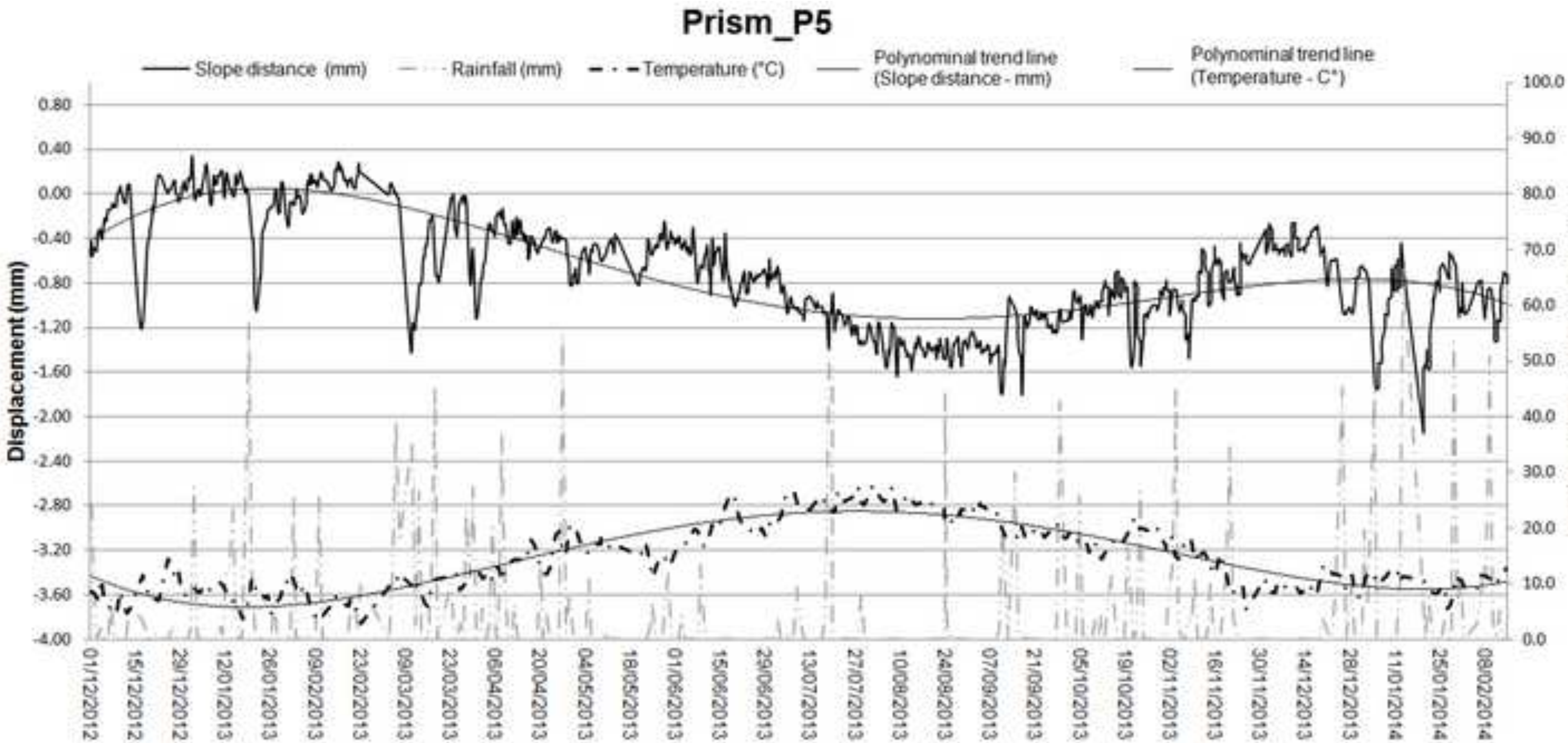

Figure 11 (Color) - 2-column

Click here to download high resolution image

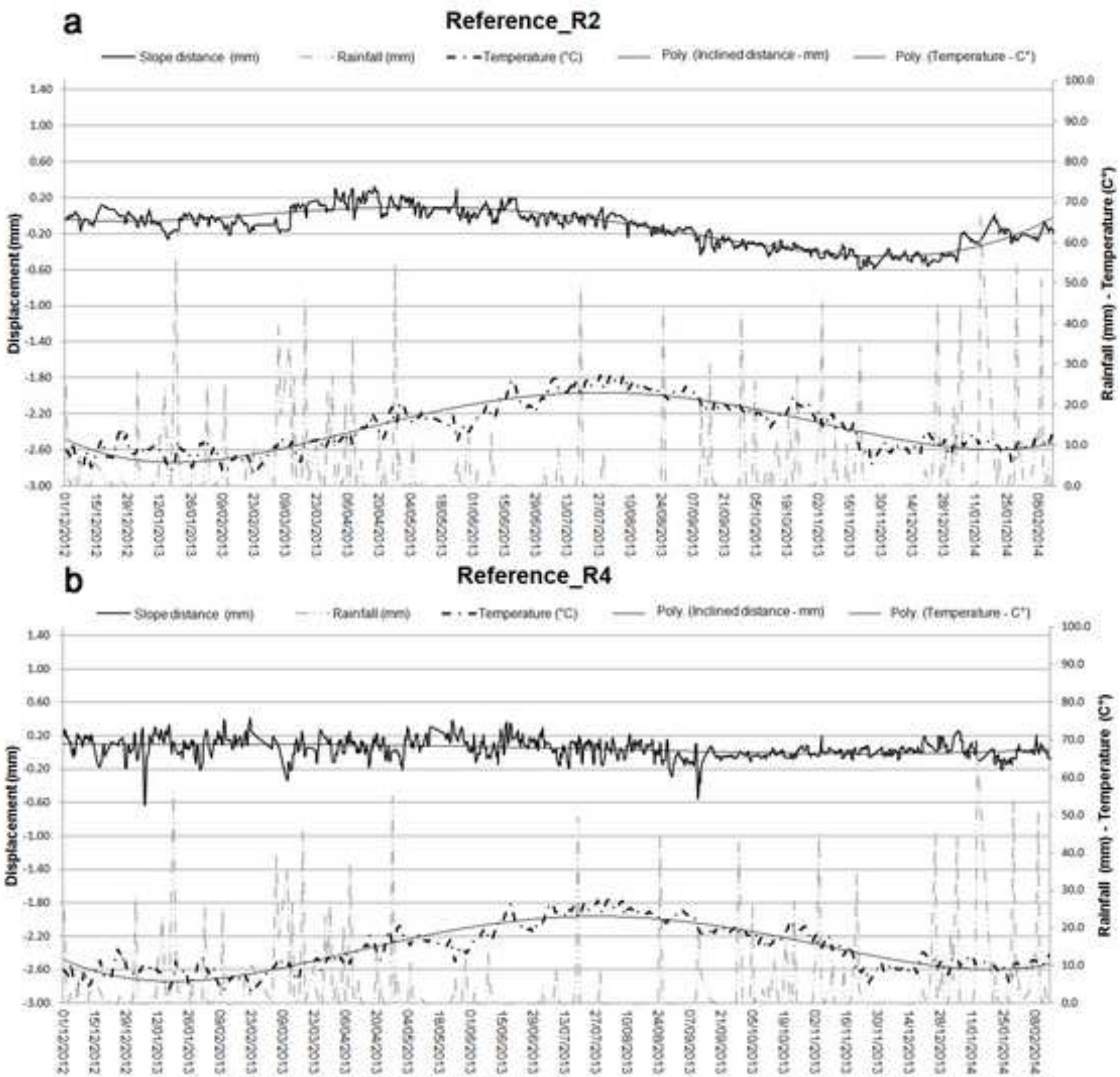

Figure 12 (Color) - 2-column

Click here to download high resolution image

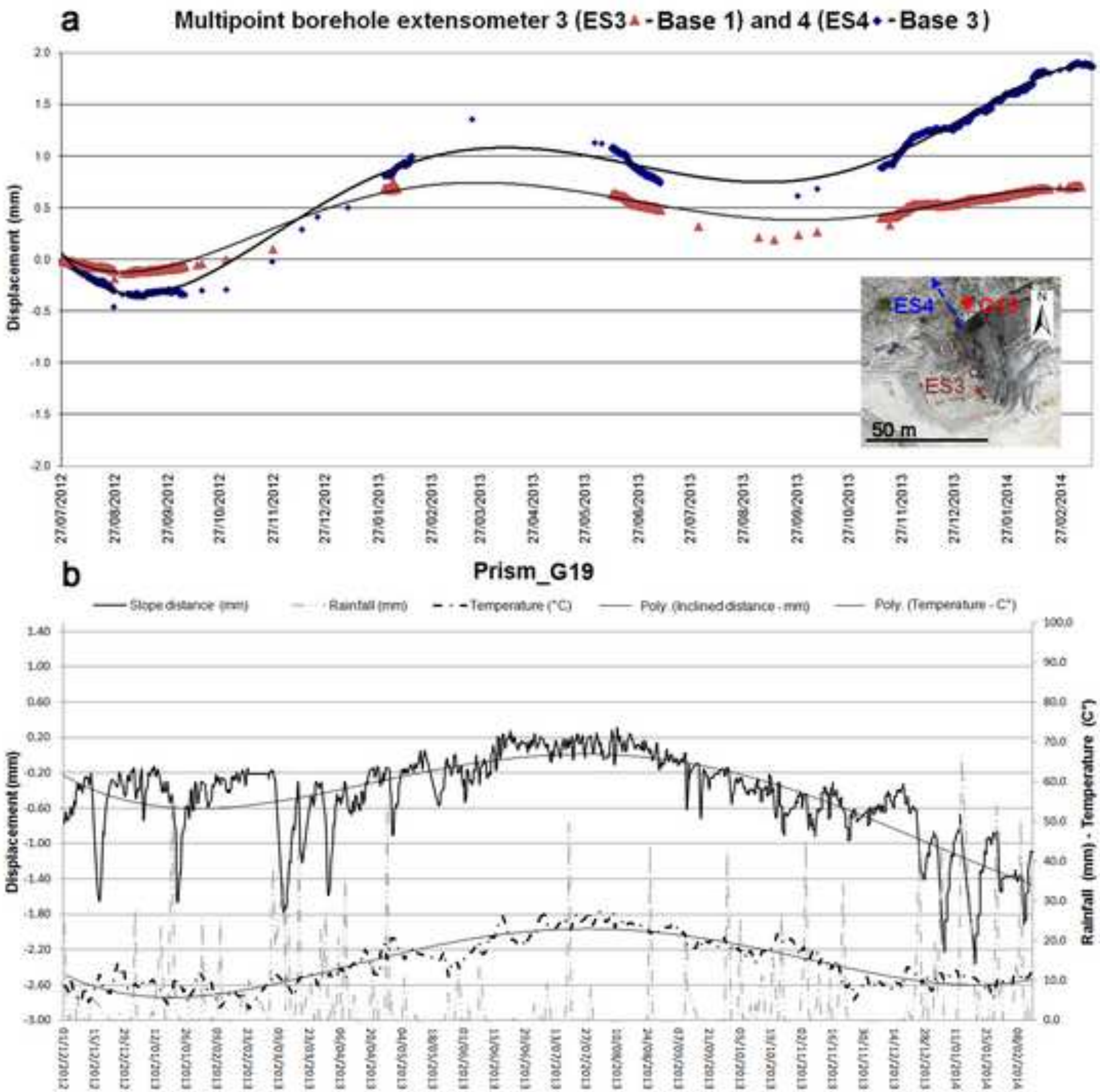

Figure 13 (Color) - 2-column
Click here to download high resolution image

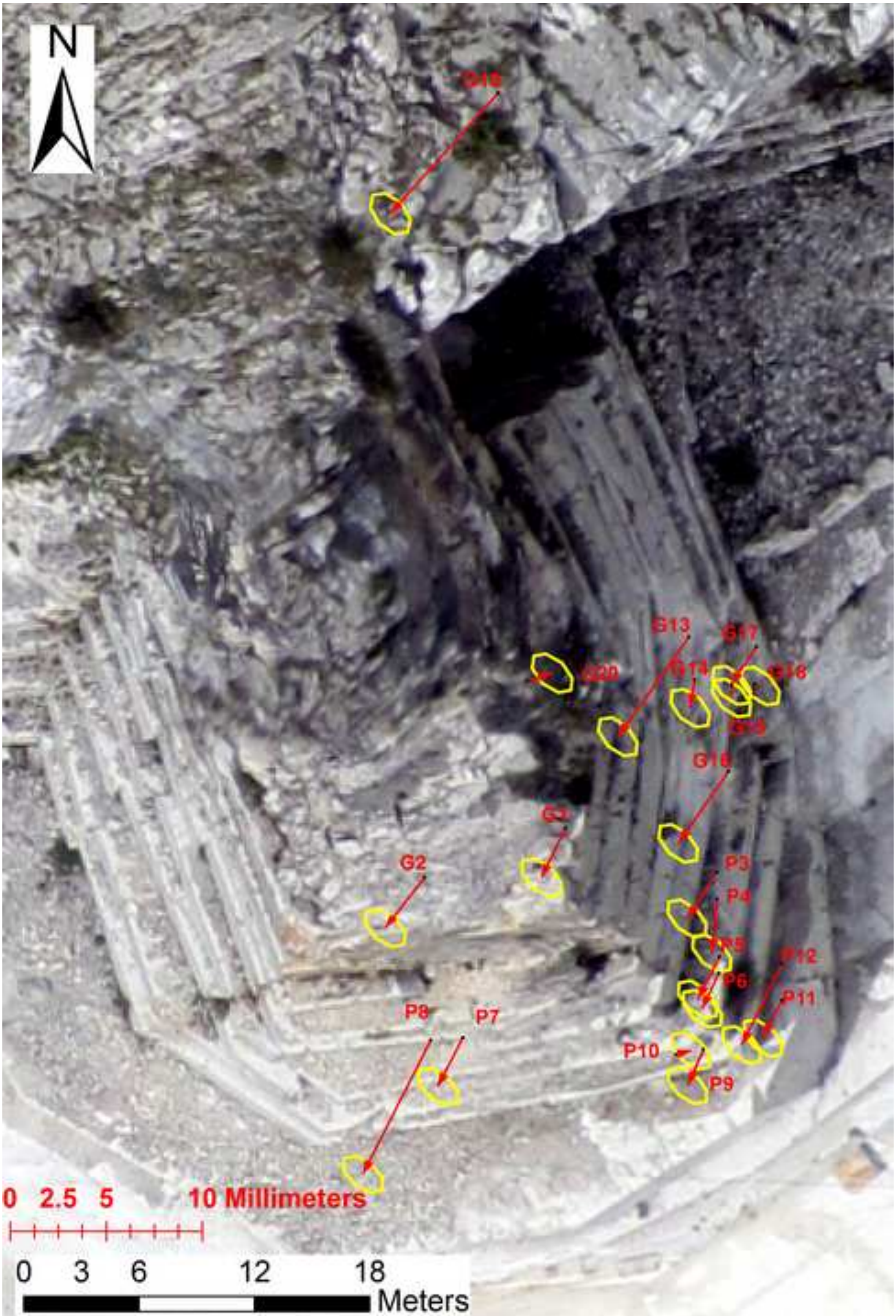

Figure 14 (Color) - single-column
Click here to download high resolution image

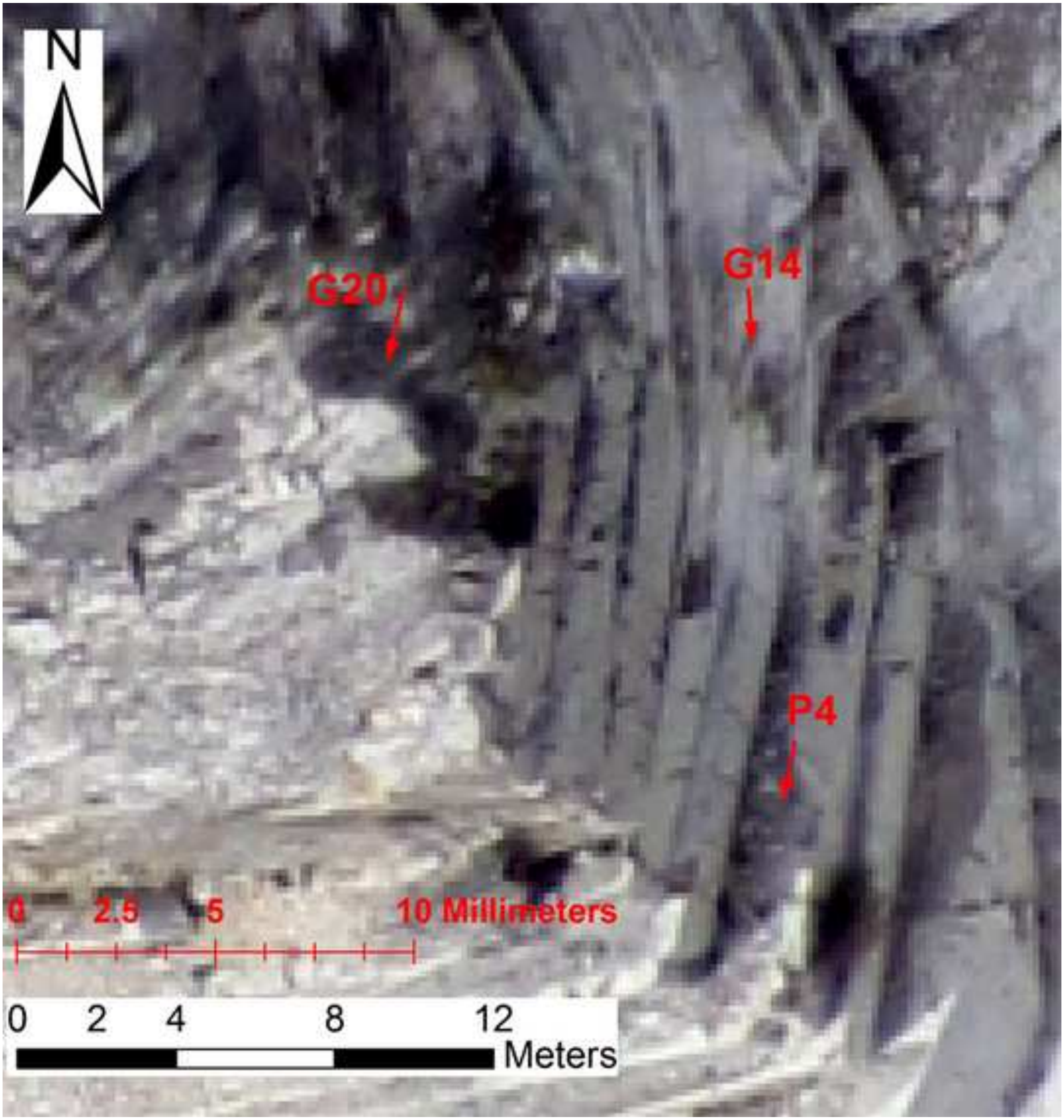

Figure 15 (Color) - 2-column

Click here to download high resolution image

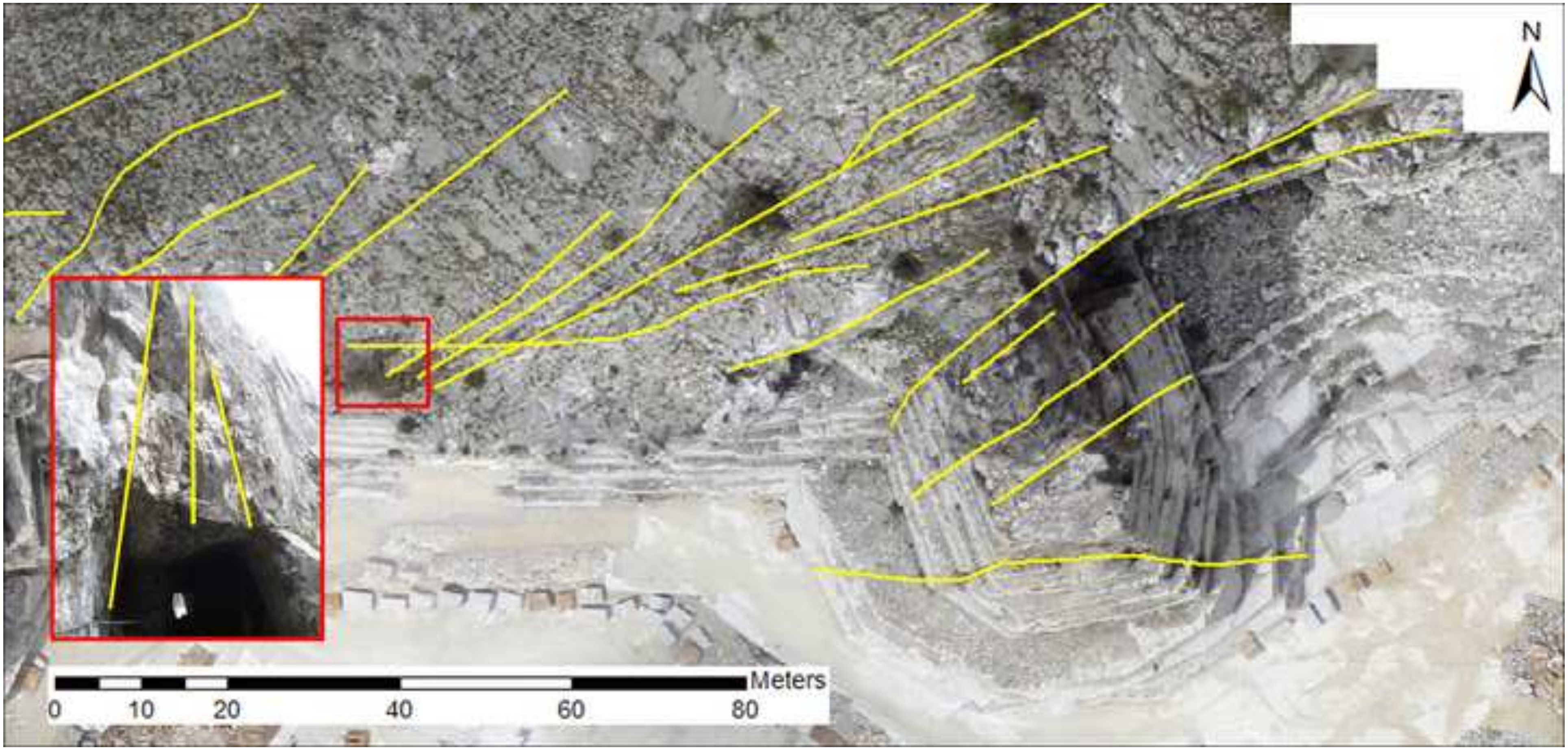

Figure 16 (Color) - single-column
Click here to download high resolution image